Measurement Based Channel Modeling with Directional Antennas for High-Speed Railways

Ruisi He[†] *, Andreas F. Molisch*, Zhangdui Zhong[†], Bo Ai[†], Jianwen Ding[†], Ruifeng Chen[†], and Zheda Li*
[†]State Key Laboratory of Rail Traffic Control and Safety, Beijing Jiaotong University, Beijing, China
*Department of Electrical Engineering, University of Southern California, Los Angeles, USA
Email: ruisi.he@ieee.org

***Abstract*—The high-speed railway propagation channel has significant effect on the design and performance analysis of wireless railway control systems. An important feature of the high-speed railway communications is the usage of directional transmitting antennas, due to which the receiver may experience strong attenuation of the line-of-sight (LOS) path under the base station (BS). This leads to a drop, and strong variations, of the signal strength under the BS. While the physical origin of the signal variations is different from conventional shadowing, it can be described by similar statistical methods. However, the effect has been largely neglected in the literature. In this paper we first define the region of the bottom of the BS, and then present a simple shadow fading model based on the measurements performed in high-speed railways at 930 MHz. It is found that the bottom area of the BS has a range of 400 m - 800 m; the standard deviation of the shadowing also follows a Gaussian distribution; the double exponential model fits the autocovariance of the shadow fading very well. We find that the directivity of the transmitting antenna leads to a higher standard deviation of shadowing and a smaller decorrelation distance under the BS compared to the region away from the BS.**

I. Introduction

High-speed railways are low-cost and environmentally friendly means of mass transportation over large distance. Wireless connectivity with the trains is essential for exchange of control and safety record information, and system such as GSM-R [1] have been developed, which are straightforward adaptations of cellular standards. However, the propagation channel in high-speed railways is significantly different from that in cellular systems because of the different location of antennas and the propagation environments. An accurate characterization of the propagation channels in high-speed railways is thus a challenging task.

Some measurement campaigns have been performed to study the propagation channels in high-speed railways [2]-[9]. However, most of the literature only investigate the effect of the environments on the channels, while another important factor of the communications - *the antennas*, has largely been neglected. An important feature of high-speed railway communications is the usage of the directional transmitting antennas. Since the practical implementation does not use the antenna sectoring in the base station (BS) to achieve omnidirectional coverage, the directional transmitter leads to poor coverage at the bottom of the BS. Fig. 1(a) shows an illustration of this effect. We can see that the high-speed train will not be in the mainlobe of the antenna when it passes under the BS (in Region 1). Due to the directivity of the BS antenna, the receiver may receive the direct path with strong attenuation even though there is no obstacle between the transmitter and receiver. In this region, the receiver is in the sidelobes of the transmitting antenna, where the received power experiences a very unusual drop and strong variations as shown in Fig. 1(b).

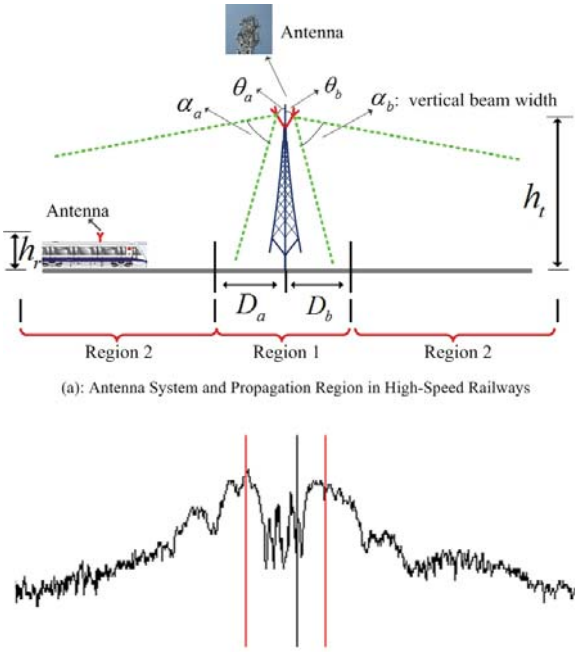

Fig. 1. (a) Antenna system and propagation region in high-speed railways. (b) A sample plot of the received power. The black vertical line represents the location of the BS and the red vertical lines represent the bottom area of the BS.

The propagation in this region, e.g., the large- and small-scale fading behaviors, should be carefully investigated. [10]-[13] analyze the small-scale fading behavior and show that the directivity of the BS antenna leads to a breakpoint distance-dependent Ricean K-factor model. However, the large-scale

This work was supported by the Fundamental Research Funds for the Central Universities under Grant 2012YJS001, 2012YJS004, and 2010JBZ008, the NSFC under Grant 61222105, and Beijing Municipal Natural Science Foundation under Grant 4112048.

978-1-4673-5939-9/13/$31.00 ©2013 IEEE

fading, also called *shadow fading*, has been largely neglected. Even though the line-of-sight (LOS) is not obstructed in this region, the reflected paths are still affected by the shadowing effects, and the weak LOS can lead to strong variation in a large-scale observed window. Even more importantly, the LOS is influenced by variations in the antenna pattern. Such variations are especially deep and rapid in the sidelobes of the pattern, which is what is "seen" when the train passes underneath the BS. Since the large-scale fading is almost independent of transmit frequency and polarization, the frequency diversity or polarization diversity are not effective to combat it [14] so that it can have a dominant performance on system performance. To the best of our knowledge, little work has been undertaken to characterize the large-scale fading with a consideration of the bottom area of the antennas in the high-speed railways.

To fill this gap, this paper presents measurements and models to define the bottom area of the directional transmitting antennas and model the shadow fading behavior. We measured the channel behavior near more than 50 BSs along a high-speed rail in China. We define the bottom area using the antenna heights and the angles between antennas and the BS tower. The propagation channel is then divided into two regions: inside and outside the bottom area. The shadow fading distribution is tested and the autocovariance is modeled using a double exponential model. The test system and measurements are introduced in Section II. The analysis and modeling of the shadow fading are presented in Section III. Finally, Section IV concludes the paper.

II. Measurement Campaign

In this section, we describe a measurement campaign for high-speed railway channels. We only give a brief summary; a more detailed description can be found in [5]-[7].

A. Test System

We carried out the 930 MHz narrowband measurements along "Zhengzhou-Xian" high-speed railway line of China. Existing GSM for rail (GSM-R) BSs were utilized as transmitters, and the broadcast control channel signal with a carrier frequency of 930 MHz was fed to a antenna as the transmission signal. The transmitting antennas were directional with 17 dBi gain and 43 dBm power. The receiver antennas were omnidirectional in azimuth and had a 4 dBi gain, mounted on top of the train. A Willtek 8300 Griffin fast measurement receiver was utilized to collect and store power data. Under the location-trigger mode, sampling of the Griffin receiver can change with the velocity of the train with the help of the distance sensor and GPS, so that the sampling interval is fixed at 10 cm no matter how fast the train moves.

B. Antenna

As shown in Fig. 1(a), the practical high-speed railway BS has two directional antennas, mounted at two angles against the BS tower (θ_a and θ_b) and pointing to each side of the BS, to achieve a line-shaped coverage along the rail track. An actual BS is shown in Fig. 2. In our measurements, three BS heights: 23, 28, and 33 m are used, and the value of θ ranges from 2^o to 7^o. The values of antenna height and θ are based on the requirements of the network design, quality of service, and practical terrains. The receiver antenna has a height of 4 m. The BSs are usually placed 15 m away from the rail track, and the coverage radius of the BS on each side is 3-4 km.

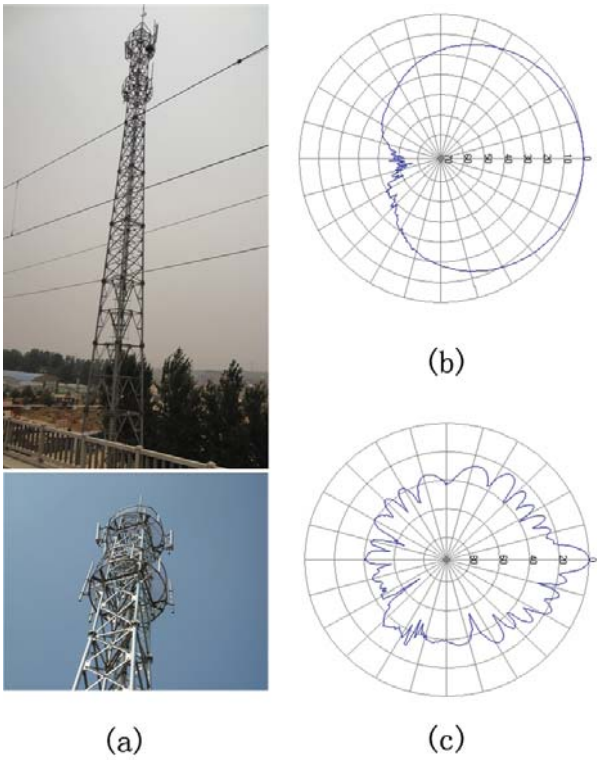

Fig. 2. (a) Overall and detailed views of the BS antenna. (b) Horizontal pattern. (c) Vertical pattern.

For the whole high-speed rail, we use the same type of transmitting antenna with 65^o horizontal and 6.8^o vertical beam widths. The nominal antenna pattern is shown in Fig. 2, though of course differences can occur from device to device. We also note that the patterns might be impacted by the mounting structures. We can see that the horizontal beam is very wide for a line-shaped coverage of rail track. Meanwhile, the mainlobe of the vertical beam α is very narrow, and the sidelobe is 20-40 dB weaker than the mainlobe. This leads to a drop, and strong variations, of the signal strength under the BS. Note that this antenna type is not a good solution for wide-area cellular coverage, however, it is reasonable for the practical implementation, e.g., reduction of costs, and convenience of producing and implementation. We stress that we used a practical and operative communication system in our measurements.

C. Measurement Environments

The measurements were carried out in 50 BSs of the high-speed railways. All of them are in the typical suburban environments where there are usually light forests and a few buildings with an average height of less than 10 m.

III. Data Analysis and Results

A. Definition of Propagation Regions

Fig. 1(b) shows that the received power experiences a very unusual drop when the train is under the BS antenna. This is due to the directivity of the transmitting antenna. Therefore, we define two regions of the propagation channels as shown in Fig. 1(a):

Region 1: where the train is under the BS, i.e., in the bottom area. In this region, the receiver may receive the direct path with strong attenuation due to the directivity of the transmitting antenna even though there is a clear LOS.

Region 2: where the train is out of the bottom area and the receiver can get a strong direct path.

Then we present the method to calculate the break point between the two regions. Fig. 3 shows a detailed view of the BS antenna system. We can see that the high-speed train enters into the mainlobe of the antenna after it passes point M. Based on the intuition, a possible definition of Region 1 in Fig. 1(a) can be written as

$$D_a + D_b = \frac{h_t - h_r}{\tan(\theta_a + \frac{\alpha_a}{2})} + \frac{h_t - h_r}{\tan(\theta_b + \frac{\alpha_b}{2})} \quad (1)$$

where h_t and h_r are the heights of the transmitter and receiver. θ_a and θ_b are the angles between antennas and the BS tower, as shown in Fig. 1(a). In our measurements $\alpha_a = \alpha_b = 6.8^{\circ}$. However, the observation based on measurements shows that point N in Fig. 3 is a more reasonable choice, which is also suggested by [15]. If we use N to define the break point between Region 1 and Region 2, the area of Region 1 can be calculated as

$$D_a + D_b = \frac{h_t - h_r}{\tan(\theta_a)} + \frac{h_t - h_r}{\tan(\theta_b)} \quad (2)$$

Fig. 4 shows that the definition of the area of Region 1 using (2) works better than (1)[1]. Eq. (2) shows that the drop and variations of the signal under the BS happen in an area larger than the area covered by sidelobe, which means this effect continues a while even when the train enters into the mainlobe. We stress that (2) comes from the statistical observation. We cannot examine the effect of α since we have fixed α for all the antennas. However, Eq. (2) works well for the practical and operative high-speed railway system.

In our measurements, the width of Region 1 ranges from 400 m to 800 m. In the following, the measurements of Region 1 and Region 2 in each BS are investigated separately and compared with each other.

B. Data Post Processing

We first use a sliding/overlapped window with an interval of 10 wavelengths and a window size of 20 wavelengths to remove the effect of the small-scale fading by averaging.

Then, we remove the effect of the distance-dependent path loss. For Region 1, since the distance-dependent attenuation is not observed[2] as shown in Fig. 1(b) and Fig. 4, we only add an offset to adjust the mean value of the signals to 0 dB. For Region 2, the log-distance model as follows is adopted to

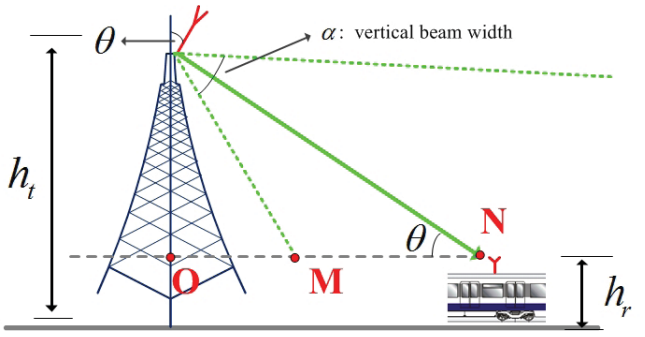

Fig. 3. Detailed view on one side of the BS antenna system in high-speed railways.

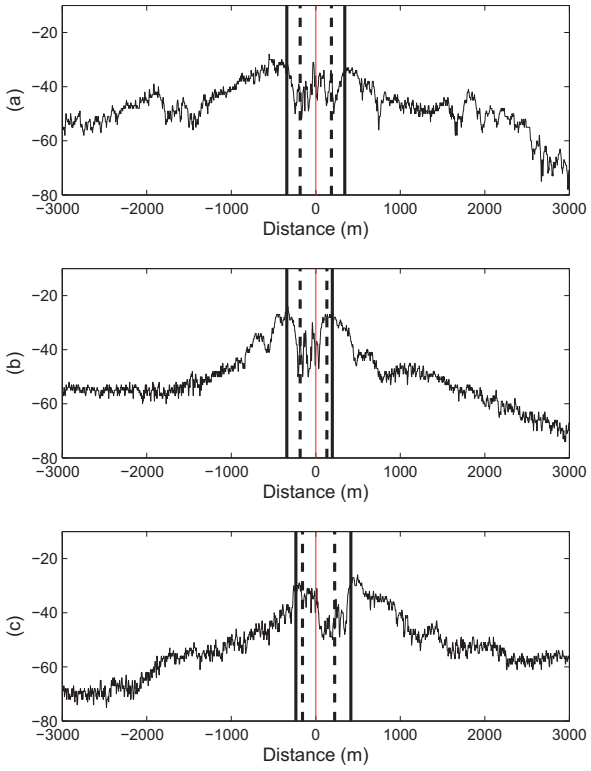

Fig. 4. Validation of Eq. (2) using the measurements in three BSs as samples. The effect of the small-scale fading has been first removed. The red vertical lines represent the locations of the BSs, the solid black vertical lines are from Eq. (2), and the dashed black vertical lines are from Eq. (1). (a): $h_t = 28$ m, $h_r = 4$ m, $\theta_a = 4^{\circ}$, $\theta_b = 4^{\circ}$. (b): $h_t = 28$ m, $h_r = 4$ m, $\theta_a = 4^{\circ}$, $\theta_b = 7^{\circ}$. (c): $h_t = 33$ m, $h_r = 4$ m, $\theta_a = 7^{\circ}$, $\theta_b = 4^{\circ}$.

[1]Measurements for other BSs were verified, though relevant plots are not shown here due to space limitations.

[2]In Region 1, the train is under the BS so that the separation distance between transmitter and receiver changes slowly when the train moves. On the other hand, the receiver can receive the signals from both of the antennas so that the distance-dependent attenuation is not distinct.

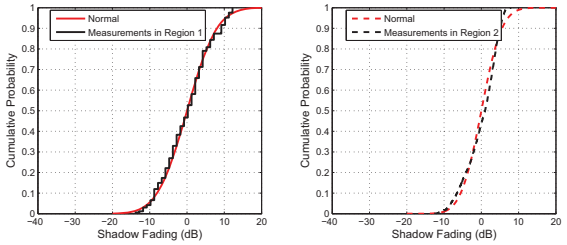

Fig. 5. Cumulative probability of the measured and lognormal-fitted shadow fading using the measurements in one BS as a sample, where $h_t = 28$ m, $h_r = 4$ m, $\theta_a = 4^{\circ}$, and $\theta_b = 4^{\circ}$.

TABLE I
PARAMETERS OF THE STANDARD DEVIATION MODEL

	μ_σ (dB)	σ_σ (dB)
Region 1	6.28	0.86
Region 2	3.48	0.67

extract the path loss *PL*

$$PL(\text{dB}) = PL_0 + 10n\log(\frac{d}{d_0}) \tag{3}$$

where *n* is the path loss exponent, d_0 is the reference distance, and PL_0 is the interception. This expression can be estimated by a linear regression using a minimum mean square error criterion.

C. Distribution of Shadow Fading

As the effects of small-scale fading and path loss are removed, the remained envelope is a random variable due to large-scale variations caused by the shadowing. Shadow fading X_σ is conventionally modeled as a lognormal distribution [14], i.e., X_σ has a zero-mean Gaussian distribution on a dB scale. We verify the measured shadow fading data by checking for Gaussian distribution of $X_\sigma(\text{dB})$. It is found that the lognormal distribution fits the shadow fading very well. Fig. 5 shows a sample plot using the measurements in one BS.

Moreover, the standard deviation $\sigma(\text{dB})$ of the shadowing is found to be a Gaussian variable from cell to cell. Thus, $\sigma(\text{dB})$ for Region 1 and 2 can be written as

$$\sigma_1(\text{dB}) = \mu_{\sigma 1} + m\sigma_{\sigma 1} \tag{4}$$

$$\sigma_2(\text{dB}) = \mu_{\sigma 2} + m\sigma_{\sigma 2} \tag{5}$$

where μ_σ is the mean value of σ; σ_σ is the standard deviation of σ; m is a zero-mean Gaussian variable of unit standard deviation $N[0,1]$. Both μ_σ and σ_σ are derived from the measurements. The values of them are given in Table I and the cumulative probability of the measured σ is shown in Fig. 6. We can see that $\mu_{\sigma 1}$ is higher than $\mu_{\sigma 2}$, and $\sigma_{\sigma 1}$ is close to $\sigma_{\sigma 2}$. A higher standard deviation in Region 1 is caused by the strong variations of the received signals in the sidelobes of the directional BS antennas.

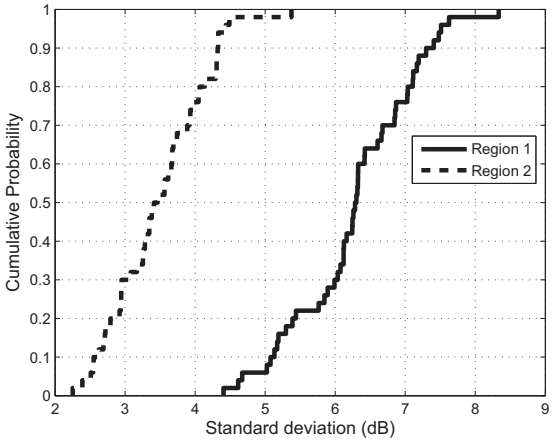

Fig. 6. Cumulative probability of the standard deviation $\sigma(\text{dB})$ based on the measurements in 50 BSs.

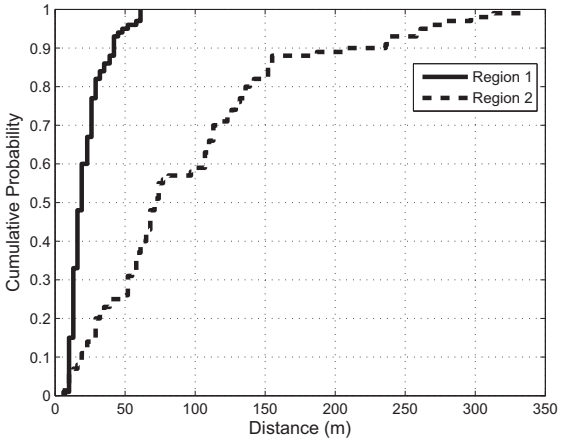

Fig. 7. Distribution of the shadow fading decorrelation distance using the measurements in the 50 BSs.

D. Correlation of Shadow Fading

We can write the spatial autocovariance of shadow fading as

$$r(\Delta d) = \frac{E\{[X_\sigma(d) - E(X_\sigma(d))][X_\sigma(d+\Delta d) - E(X_\sigma(d+\Delta d))]\}}{\sqrt{Var[X_\sigma(d)]}\sqrt{Var[X_\sigma(d+\Delta d)]}} \tag{6}$$

where d is the distance and Δd is the separation distance. $E[\cdot]$ and $Var[\cdot]$ denote the expected value and the variance of $[\cdot]$ respectively. The measured autocovariance of shadowing is obtained for each BS and then compared with each other. We define the decorrelation distance d_c as the minimum separation distance that satisfies the equation $r(\Delta d) \leq 0.5$. Based on the measurements in each BS, the distribution of shadow fading decorrelation distance is shown in Fig. 7. The plot shows that the decorrelation distance for Region 1 is significantly smaller than for Region 2. The mean value of the decorrelation distance d_c for Region 1 is 22 m, while it is 96 m for Region 2. The higher value of d_c for Region 2 is caused by the dominant LOS path.

TABLE II
PARAMETERS OF THE DOUBLE EXPONENTIAL MODEL

	α	d_1 (m)	d_2 (m)
Region 1	0.86	22.74	8741
Region 2	0.30	13.33	232.7

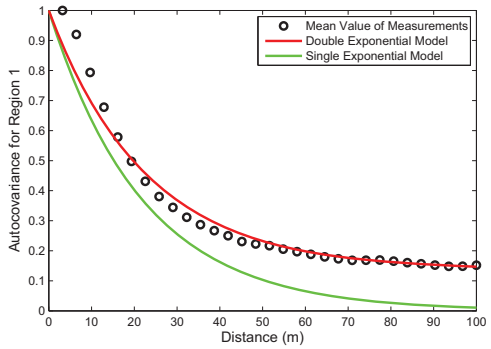

Fig. 8. Measured autocovariance in all 50 BSs and models according to (7) and (8) for Region 1.

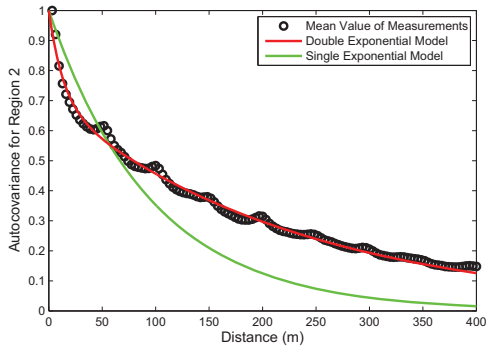

Fig. 9. Measured autocovariance in all 50 BSs and models according to (7) and (8) for Region 2.

Fig. 8 and 9 show the averaged curves of the measured autocovariances in all 50 BSs. It can be observed that the autocovariance decays faster for Region 1 than for Region 2. We can then model the autocovariance of shadow fading by some well known analytical models, see [16] and the references therein. All the autocovariance models are expressed as a function of distance. The most common autocovariance model is the *Single Exponential Model*:

$$r(\Delta d) = \exp(-\frac{\Delta d}{d_c}) \tag{7}$$

where d_c is the decorrelation distance. The sum of two independent exponential processes, the *Double Exponential Model*, is also widely used:

$$r(\Delta d) = \alpha \exp(-\frac{\Delta d}{d_1}) + (1-\alpha)\exp(-\frac{\Delta d}{d_2}) \tag{8}$$

where $0 \leq \alpha \leq 1$, $d_1 > 0$, and $d_2 > 0$ are the tunable parameters. Both of the models are tested by our measurements, as shown in Fig. 8 and 9. The *Double Exponential Model* is found to fit very well. The tunable parameters of the *Double Exponential Model* for Region 1 and 2 are summarized in Table II.

IV. CONCLUSION

In this paper, the shadow fading behavior in high-speed railways using the directional transmitting antennas is investigated. We divide the propagation channel into two regions: Region 1 - inside the bottom area of the antenna; and Region 2 - outside the bottom area of the antenna. Then we present a simple shadow fading model based on the measurements. It is found that Region 1 has a range of 400 m - 800 m under the BS. The large-scale fading in the two regions both follow the lognormal distribution, and the double exponential model fits the autocovariance of shadow fading very well. The standard deviation of shadowing is found to follow a Gaussian distribution, with a mean value of 6.28 dB for Region 1 and 3.48 dB for Region 2. The decorrelation distance is 22 m for Region 1 and 96 m for Region 2. We can see that the directivity of the transmitter leads to a smaller standard deviation of shadowing and a higher decorrelation distance for Region 2.

REFERENCES

[1] Z. Zhong, X. Li, and W. Jiang, *Principles and Foundation of Integrated Digital Mobile Communicationsystem for Railway*, 2003.

[2] M. Goller, "Application of GSM in high speed trains: measurement and simulations," *IEE Colloquium on Radio communications in Transportation*, pp. 5/1-5/7, 1995.

[3] J. Qiu, C. Tao, L. Liu, and Z. Tan, "Broadband channel measurement for the high-speed railway based on WCDMA," in *Proc. IEEE VTC*, Japan, 2012, pp. 1-5.

[4] M. Uhlirz, "Adapting GSM for use in high-speed railway networks," *Dissertation for Institut fiir Nachrichtentechnik und Hochfrequenztechnik Technische Universitiit Wien*, 1995.

[5] R. He, Z. Zhong, B. Ai, L. Xiong, and H. Wei, "A novel path loss model for high-speed railway viaduct scenarios," in *Proc. IEEE WiCOM*, China, 2011, pp. 1-4.

[6] R. He, Z. Zhong, B. Ai, and J. Ding, "An empirical path loss model and fading analysis for high-speed railway viaduct scenarios," *IEEE Antennas Wireless Propag. Lett.*, vol. 10, pp. 808-812, 2011.

[7] R. He, Z. Zhong, B. Ai, and J. Ding, "Propagation measurements and analysis for high-speed railway cutting scenario," *Electron. Lett.*, vol. 47, no. 21, pp. 1167-1168, Oct. 2011.

[8] H. Wei, Z. Zhong, L. Xiong, B. Ai, and R. He, "Study on the shadow fading characteristic in viaduct scenario of the high-speed railway," *Proc. IEEE Chinacom*, China, 2011.

[9] P. Kyosti *et al.*, "WINNER II channel models," *WINNER II Public Deliverable*, Sept. 2007.

[10] R. He, Z. Zhong, B. Ai, and J. Ding, "Measurements and analysis of short-term fading behavior for high-speed rail viaduct scenario," in *Proc. IEEE ICC*, Canada, 2012, pp. 4563-4567.

[11] R. He, Z. Zhong, B. Ai, G. Wang, J. Ding, and A. F. Molisch, "Measurements and analysis of propagation channels in high-speed railway viaducts," *IEEE Trans. Wireless Commun.*, to appear.

[12] R. He, Z. Zhong, B. Ai, J. Ding, Y. Yang, and A. F. Molisch, "Short-term fading behavior in high-speed railway cutting scenario: measurements, analysis, and statistical models," *IEEE Trans. Antennas Propag.*, to appear.

[13] R. He, Z. Zhong, B. Ai, J. Ding, and Y. Yang, "Propagation measurements and analysis of fading behavior for high speed rail cutting scenarios," in *Proc. IEEE Globecom*, USA, 2012, pp. 5237-5242.

[14] A. F. Molisch, *Wireless Communications*. 2nd Edition. IEEE-Wiley, 2011.

[15] R. He, Z. Zhong, B. Ai, and J. Ding, "Measurements and analysis of the directional antenna bottom area in high speed rail," in *Proc. IEEE Int. Symp. Antennas Propag.*, USA, 2012, pp. 1-2.

[16] S. S. Szyszkowicz, H. Yanikomeroglu, and J. S. Thompson, "On the feasibility of wireless shadowing correlation models," *IEEE Trans. Veh. Technol.*, vol. 59, no. 9, pp. 4222-4236, 2010.